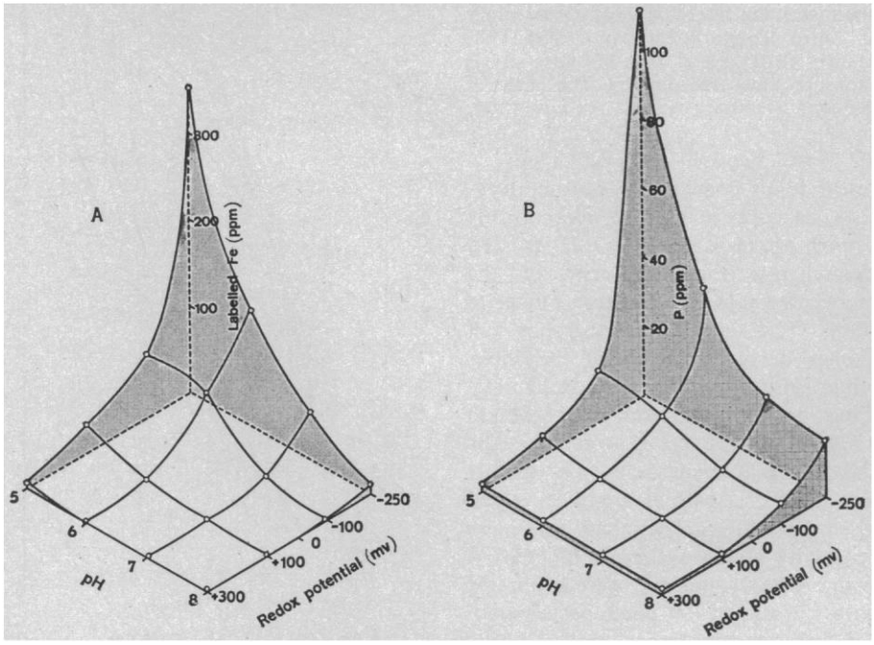

Fig. 1. (A) Release of labeled iron from strengite in flooded soil at various redox potential–*p*H combinations. The total amount of iron added as strengite was 598 parts per million (ppm). (B) Phosphate extracted from flooded soil at various redox potential–*p*H combinations; *P* represents both the phosphate added as strengite and the native soil phosphate. The total amount of phosphate added as strengite was 332 ppm. The original phosphate content of the soil was 182 ppm.

potential showed a similar trend: at the lowest redox potential (denoting highly reducing conditions), a decrease in *p*H resulted in a large increase in the amounts of iron and phosphate dissolved, whereas under more oxidizing conditions (higher redox potentials) *p*H had much less effect on the amounts of iron and phosphate dissolved. Tanaka *et al.* (*5*) attributed most of the increase in phosphate solubility after soil submergence to the increase in *p*H which usually occurs when acid soils are flooded. On the contrary, our results show that in reduced soils under conditions where *p*H was carefully regulated, increases in *p*H resulted in the release of smaller amounts of phosphate. The dissolution of strengite with the production of Fe^{2+} and $H_2PO_4^-$ which occurred as both *p*H and redox potential were decreased suggests that strengite dissolution in flooded soils may be described by the following equation:

$$FePO_4 \cdot 2H_2O + 2H^+ + e^- \rightleftharpoons Fe^{2+} + H_2PO_4^- + 2H_2O$$

$$E_H = E^\circ - 0.059 \log [Fe^{2+}] - 0.059 \log [H_2PO_4^-] - 0.118\ pH$$

where E_H represents the potential for the reversible reaction and E° is the potential when all substances are at unit activity. The ferrous phosphate produced probably remains in an amorphous form, since crystalline ferrous phosphate (vivianite) is extremely insoluble.

More intensive reducing conditions are apparently required to reduce strengite chemically than to bring about its microbial reduction. In a study of strengite dissolution in a chemical system, Williams and Patrick (*11*) found that in cases where nascent hydrogen was used as a reducing agent a redox potential of −290 mv was required at *p*H 5 to reduce and solubilize strengite. At higher *p*H values no more than a trace of strengite was reduced even at more negative redox potentials. Microbial enzyme systems that function in a flooded soil are apparently effective in lowering the activation energy required for strengite reduction with the result that there is a shift in the critical redox potential to a higher value.

The results of this study show that strengite partially dissolves under reducing conditions such as those that exist in flooded soils deprived of oxygen. A close relationship existed between the amount of strengite dissolved and both the redox potential and the *p*H of the soil suspension. There is a marked interaction between acidity and redox potential, with strengite reduction and solubilization being more pronounced under conditions of low *p*H combined with low redox potential.

W. H. Patrick, Jr.
S. Gotoh*
B. G. Williams†
Agronomy (Soils) Department,
Louisiana State University,
Baton Rouge 70803

References and Notes

1. M. Aoki, *J. Sci. Soil Manure Tokyo* **15**, 182 (1941).
2. R. L. Beacher, paper presented at the Fifth Meeting of the Working Party on Fertilizers, Malaya [*Food Agr. Organ. Int. Rice Comm. Background Pap.* (1955)]; R. E. Shapiro, *Soil Sci.* **85**, 190 (1958).
3. E. Eriksson, *J. Soil Sci.* **3**, 238 (1952).
4. D. B. Bradley and D. H. Sieling, *Soil Sci.* **76**, 175 (1953).
5. A. Tanaka, N. Watanabe, Y. Ishizuka, *J. Sci. Soil Manure Tokyo* **40**, 406 (1969).
6. W. H. Patrick, Jr., *Nature* **212**, 1278 (1966).
7. W. E. Cate, E. O. Huffman, M. E. Deming, *Soil Sci.* **88**, 130 (1959).
8. A sample of strengite synthesized by Cate *et al.* (*7*) was kindly supplied by J. R. Lehr, Tennessee Valley Authority, Muscle Shoals, Alabama.
9. K. Kumada and T. Asami, *Soil Plant Food* **3**, 197 (1958).
10. S. C. Chang and M. L. Jackson, *Soil Sci.* **84**, 133 (1957).
11. B. G. Williams and W. H. Patrick, Jr., *Nature Phys. Sci.* **234**, 16 (1971).

* On leave from the Kyushu Agricultural Experiment Station, Ministry of Agriculture and Forestry, Chikugo, Fukuoka Prefecture, Japan.
† On leave from the Division of Land Research, Commonwealth Scientific and Industrial Research Organisation, Darwin, Australia.

4 October 1972; revised 22 November 1972

Comet Bennett 1970 II

Abstract. *The model for dust comets, formulated by Finson and Probstein, which had previously been tested only on Comet Arend-Roland 1957 III, has been successfully applied to three calibrated photographic plates of Comet Bennett. The size distribution, emission rate, and initial velocities of dust particles emitted from the comet's nucleus are given.*

Comet 1970 II, discovered at Riviera, South Africa, by J. C. Bennett on 28 December 1969, became a spectacular object visible to the naked eye in the spring of 1970 when it displayed a straight narrow plasma tail and a huge moderately curved dust tail. With the use of photographic plates sensitive only in certain parts of the spectrum (particularly in the red region) and with

Fig. 1. Dust tail of Comet Bennett photographed at the Inter-American Observatory at Cerro Tololo, Chile, on 18.36 U.T. March 1970. Plate 103a-F; filter RG1; exposure time, 15 minutes. The scale of the copy is 160 arc seconds per millimeter.

appropriate filters, the plasma tail can be completely suppressed (Fig. 1). The structure of a dust tail on such plates was shown by Finson and Probstein (*1*) to contain astrophysically significant information about the nature of the dust and gas production mechanisms in comets.

In the Finson-Probstein model of dust comets it is assumed that there is an essentially continuous emission of solid particles of various sizes from the nucleus into the atmosphere brought about by the drag forces of the outgoing gas. Shortly after the ejection of solid particles, the solar gravity and solar radiation pressure are considered to be the only two forces that control the motion of the dust particles in the cometary tail. The trajectory of any individual particle depends on its size and on the time, velocity, direction, and other circumstances of ejection. The observed photometric profile of the tail at any time depends on three parametric functions, namely, the size distribution of the ejected particles, their emission rate as a function of time before the time of observation, and variations in the initial particle velocity with time and size. The photometric profile also depends on the geometrical configuration of the sun, earth, and comet in space.

The Finson-Probstein model is believed to be one of the most effective methods yet applied in the physical research on comets. Heretofore, however, it has been used to analyze only Comet Arend-Roland 1957 III (*1*). To demonstrate the superiority of the model, Sekanina applied the model to three high-quality photographs of Comet Bennett, secured at the Inter-American Observatory at Cerro Tololo, Chile, between 10 March and 18 March 1970. The three plates were taken by the Curtis-Schmidt telescope (61/91 cm, *f*/3.5) as part of a project supervised by Miller. They had maximum sensitivity at a wavelength of 6600 Å with an RG1 filter and were calibrated with the use of 14 photometric spots. The observations were made shortly before the comet reached the perihelion point on 20.0 March U.T. (universal time), when it was 0.538 astronomical unit from the sun. Sekanina carried out the absolute calibration of the plates, using the surface brightness of the night-sky background.

In practice, the crucial point of the Finson-Probstein method is to reach the best possible agreement between the observed photometric profile of the comet's tail and a theoretical surface density distribution by varying the three parametric functions by trial and error. For a particular combination of the three parametric functions the corresponding surface density distribution can be obtained either by calculating contributions from particles of various sizes ejected with the times held constant and then integrating the contributions over all ejection times (synchrone approach) or by calculating contributions from particles of constant dimensions ejected at various times and then integrating the contributions over all particle sizes (syndyne approach).

In the case of Comet Bennett we have used the synchrone approach, and a very satisfactory agreement between the theory and observations (for example, see Fig. 2) has given the following detailed results on the comet's behavior and structure:

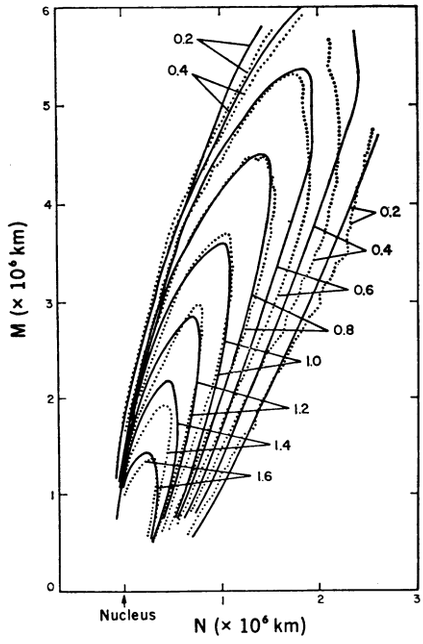

Fig. 2. Comparison of the observed isophotes (dotted curves) with the theoretical density distribution (solid curves) for the photograph taken on 18 March 1970 (see Fig. 1). The numbers at individual pairs of curves indicate the logarithm of the relative surface density; *M* is the direction of the radius vector projected on the photographic plane; *N* is perpendicular to *M* in the direction of increasing right ascension (to the right).

1) The normalized size-density distribution function of the emitted dust particles $g(\rho d)$ [where ρ is the density of a particle (in grams per cubic centimeter) and d is its diameter (in centimeters)] is shown in Table 1. This distribution has a sharp maximum at $\rho d = 1.12 \times 10^{-4}$ g cm^{-2}, and the optically representative particle diameter is $2.06 \times 10^{-4}\ \rho^{-1}$ cm.

2) The emission rate of the dust, $\dot{m}_d$ (in grams per second), is inversely proportional to the particle albedo. For an assumed value of the particle albedo of 0.1 we find

$$\dot{m}_d = 4.5 \times 10^{4}\ \delta r^{-12} \text{ for } -45 \text{ days} \leqq t < -13 \text{ days}$$

$$\dot{m}_d = 9.3 \times 10^{6}\ \delta r^{-1} \text{ for } -13 \text{ days} \leqq t < -1.7 \text{ days}$$

where $\delta = 0.5$ for -17 days $< t < -10$ days and $\delta = 1$ elsewhere. Here the time t (in days) from the passage through perihelion is related to the heliocentric distance, r (in astronomical units), by

$$t = 27.4\ (r + 1.075) \cdot (r - 0.538)^{1/2}$$

Table 1. Normalized size-density distribution function of the emitted dust particles.

$g(\rho d)$	For ρd (g cm^{-2})
$2.1 \times 10^{-14}\ (\rho d)^{-5}$	$\geqq 36 \times 10^{-4}$
$5.8 \times 10^{-12}\ (\rho d)^{-4}$	2.6×10^{-4} to 36×10^{-4}
$8.9 \times 10^{-12}\ (\rho d)^{-5}\ (\rho d - 0.9 \times 10^{-4})$	0.9×10^{-4} to 2.6×10^{-4}
0	$< 0.9 \times 10^{-4}$

Although no effect of particle ejection from times earlier than 45 days before perihelion could be detected, the dust emission rate nearer the perihelion became apparently large enough to dim the solar illumination of the nucleus.

3) Initial particle velocities, v_d (in kilometers per second), can be approximated by

$$v_d = \frac{0.80}{1 + 0.38\, r\, (1 - \mu)^{-1/2}}$$

where $1 - \mu$ is the particle acceleration caused by the solar radiation pressure (in units of the solar gravity). Comparison of the observed v_d with that predicted in Probstein's theory (*2*) indicates that the drag force must have essentially been due to water vapor, that the ratio of the rate of emission of dust to the rate of emission of gas at the time of observations was about 0.5, and that the radius of the nucleus of Comet Bennett was about 2.6 km. Furthermore, the production rate of molecules with a molecular weight of 18 at 1 astronomical unit from the sun (extrapolated from the working solar distance of ~ 0.6 astronomical unit with the use of the r^{-2} law) is 4×10^{17} molecule cm^{-2} sec^{-1}, which compares most favorably with the theoretical rate of vaporization of water snow, calculated from the energy balance equation (*3*).

Z. SEKANINA
Smithsonian Astrophysical Observatory, Cambridge, Massachusetts 02138
F. D. MILLER
Department of Astronomy, University of Michigan, Ann Arbor 48104

References and Notes

1. M. L. Finson and R. F. Probstein, *Astrophys. J.* **154**, 327 (1968); *ibid.*, p. 353.
2. R. F. Probstein, in *Problems of Hydrodynamics and Continuum Mechanics* (Society for Industrial and Applied Mathematics, Philadelphia, 1969), p. 568.
3. A. H. Delsemme and D. C. Miller, *Planet. Space Sci.* **19**, 1229 (1971); B. G. Marsden, Z. Sekanina, D. K. Yeomans, *Astron. J.*, in preparation.
4. One of us (Z.S.) thanks Prof. R. F. Probstein, Department of Mechanical Engineering, Massachusetts Institute of Technology, and Dr. M. L. Finson, Avco-Everett Research Laboratory, Everett, Massachusetts, for most helpful discussions; Prof. F. L. Whipple and Dr. A. F. Cook, Smithsonian Astrophysical Observatory, for a few additional comments and suggestions; Dr. B. G. Marsden, Smithsonian Astrophysical Observatory, for providing the osculating orbit and detailed ephemeris of the comet; R. H. Johnson, PhotoMetrics, Inc., Lexington, Massachusetts, for the high-quality isophotometric tracings of the plates; and Mrs. S. K. Rosenthal, Smithsonian Astrophysical Observatory, for programming assistance. This work was made possible by grant NGR 09-015-159 from the National Aeronautics and Space Administration. The observing project under which one of us (F.D.M.) took the photographic plates of the comet was supported by a grant from the National Science Foundation.

19 October 1972

Isocyanate Intermediates in Ammonia Formation over Noble Metal Catalysts for Automobile Exhaust Reactions

Abstract. *Isocyanate species have been detected on the surface of noble metal catalysts during the reactions of carbon monoxide with nitric oxide. The intensity of the surface isocyanate infrared band correlates with the known ammonia-forming tendencies among the noble metals. The discovery of this isocyanate species suggests a new mechanistic pathway to the ammonia formed during catalytic reduction of nitrogen oxides in automobile exhaust.*

Recent interest in the chemistry of nitric oxide reduction in automotive exhaust gas (*1–3*) has prompted study of the infrared spectra of species adsorbed on the surface of noble metal catalysts during the reaction of NO with CO. When reaction mixtures of CO, NO, and N_2 were contacted with catalysts consisting of noble metals on alumina at elevated temperatures, very strong infrared absorption bands were observed in the region from 2260 to 2270 cm^{-1}. After a number of auxiliary experiments, including some in which ^{15}NO was used, it was concluded that these intense bands are due to

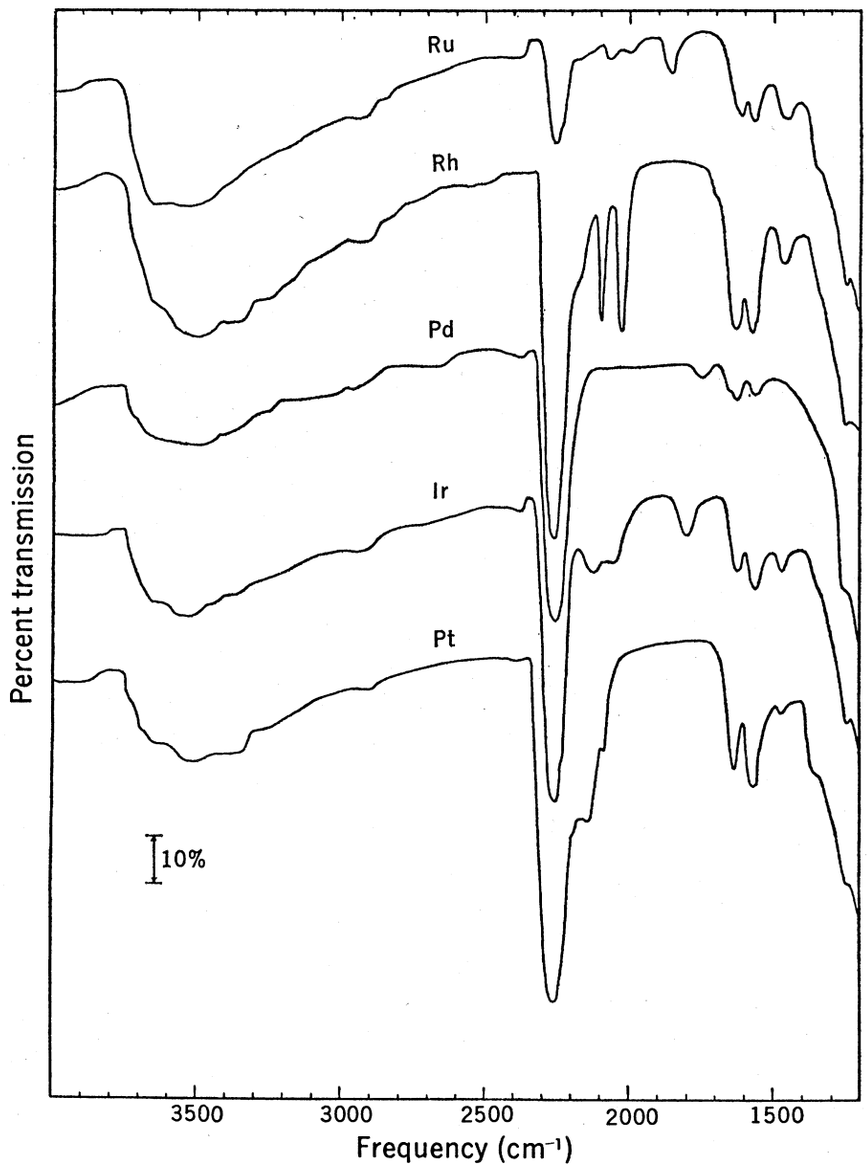

Fig. 1. Spectra observed at room temperature and a pressure of 1 torr after dosing the clean sample of noble metal (5 percent) on Al_2O_3 with 100 torr of a blend containing CO (10 percent), NO (5 percent), and N_2 (85 percent) at 400°C.